Society of Naval Architects and Marine Engineers Annual Meeting, Ottawa, 15-18 October 1997

MOTIONS AND LOADS OF A HYDROELASTIC FRIGATE MODEL IN SEVERE SEAS

Kevin McTaggart (M), Defence Research Establishment Atlantic, Dartmouth, Nova Scotia
Indranath Datta (M), Institute for Marine Dynamics, St. John's, Newfoundland
Alasdair Stirling (M), UK Ministry of Defence, Helensburgh, Scotland
Stephen Gibson (M), UK Ministry of Defence, Helensburgh, Scotland
Ian Glen (M), Fleet Technology Limited, Kanata, Ontario

Abstract

The design of a warship requires accurate predictions of sea loads in extreme wave conditions. Such loads are difficult to obtain from full scale measurements alone because the durations over which these conditions exist are short relative to the overall operational profile of the ships, and a captain will make every effort to minimize these loads in normal operational circumstances. In response to a requirement for data on ship structural behaviour in severe seas, a segmented flexible backbone model of a modern Canadian frigate was built and tested in severe regular and irregular wave conditions. Linear frequency domain predictions are shown to give good agreement with experimental wave-induced oscillatory motions and sea loads up to the maximum tested wave steepness of 1/15. Nonlinear effects induce non-zero mean vertical bending moment at midships, leading to sag/hog ratios significantly greater than unity. Analysis of measured whipping responses in regular waves demonstrates that the induced vertical bending moment at midships can approach the wave-induced oscillatory moment in magnitude at higher operating speeds and wave steepnesses.

NOMENCLATURE

A^S	shear area
A^S_h	horizontal shear area
A^S_v	vertical shear area
AP	aft perpendicular
a	wave amplitude
B	ship beam
BL	baseline
CG	center of gravity
E	elastic modulus
Fn	Froude number
FP	forward perpendicular
G	shear modulus
$\overline{GM}$	metacentric height
g	gravitational acceleration
H	wave height
H_s	significant wave height
I^A	second moment of structural area
I^A_{yy}	vertical second moment of structural area
I^A_{zz}	horizontal second moment of structural area
$\overline{KG}$	height of center of gravity above keel
k	wavenumber
k_r	sectional gyradius proportionality constant
$\overline{kg_i}$	height of sectional CG above keel
L	length between perpendiculars
L_{oa}	length overall
LCG	longitudinal center of gravity
l_i	sectional length
m_i	sectional mass
m_0	area under spectrum
n_w	whipping cycles per wave encounter
r_{xx}	ship roll gyradius
r_{xx-i}	section roll gyradius about section CG
r_{yy}	ship pitch gyradius
T	draft at midships
T_p	peak wave period
T_4	roll natural period in water
t_s	time of slamming
V_i	wave-induced oscillatory load
V'_i	dimensionless oscillatory load
$\overline{V}^S_5$	mean still-water vertical moment
$\overline{V}^U_5$	mean vertical moment due to ship speed
$\overline{V}^W_5$	mean vertical moment due to waves
$\overline{V}^{W\prime}_5$	dimensionless mean moment due to waves
V^{hog}_5	hog bending moment
V^{sag}_5	sag bending moment
V^w_5	whipping bending moment
$\hat{V}^w_5$	maximum whipping bending moment
$\hat{V}^{w\prime}_5$	dimensionless max. whipping moment
β_s	sea direction (180 degrees in head seas)
ζ_i	motion amplitude
ζ'_i	dimensionless motion amplitude
λ	wavelength or scaling factor
ξ_w	whipping damping coefficient
ρ	water density
ω	wave frequency
ω_w	whipping frequency
$\triangle$	ship mass displacement

INTRODUCTION

The designers of ships have always had to wrestle with the difficulties of determining suitable loads for structural design. Before the availability of modern computers, standard wave heights such as $L/20$ or $1.1\sqrt{L}$ (L having units of feet) were adopted not because they represented waves that a ship would encounter, but rather as waves that could cause representative stresses in a midship section. In comparison to other industries, there has been relatively little monitoring of operational ships to establish actual in-service loads and responses. Among the major difficulties have been logistics, inaccessibility to scientific personnel, problems with automating the data acquisition process, training of onboard personnel to acquire data, and monitoring instrumentation integrity.

Warships present particular challenges for designers because of the requirement to withstand severe seas for extended periods of time without significant weather damage. Numerical simulations and model tank tests are practical alternatives to full scale measurements for determining design loads. Advances in both theory and computing power are enabling naval architects to predict loads in extreme conditions. However, there has always been difficulty in verifying numerical models by full scale trials data due to uncontrolled conditions. Another factor which limits the usefulness of full scale trials data is that measurements of wave conditions are often unreliable.

The theory and practical application of wave tank model testing is well established; however, determination of structural loads presents requirements additional to normal resistance and seakeeping tests. Like resistance and seakeeping tests, hydrodynamic load tests require a geosim of the ship with Froude scaling. The dependence of hydrodynamic loads on ship girder deflections requires that the model must also represent the flexural properties of the ship.

BACKGROUND

The Canadian Navy utilizes the following resources to predict rational design loads for its ships:

- full scale trials at sea (in addition to dedicated short-term trials, strain measurement systems are installed on operational navy ships to obtain long-term data),
- numerical simulation software,
- model tests.

A series of long term instrumentation packages has been fitted to Canadian naval ships to measure long term strains; however, in peacetime ship captains will avoid severe seas or change course and speed to minimize the effects of severe seas. Furthermore, the lack of simultaneous measurements of wave conditions limits the usefulness of the long term strain data for validation of numerical simulation software.

To date, numerical simulations of sea loads on Canadian naval vessels have been largely limited to frequency domain predictions using strip theory and three dimensional codes. Transient loads and hydroelastic effects have been largely neglected; thus, wave-induced loads have only been considered at the encounter frequencies of wave spectral components. For the design load case of a ship in severe seas, the assumptions of linearity in most frequency domain codes can introduce significant errors.

The Canadian Navy plans to develop more sophisticated codes for prediction of ship design loads. A major consideration in the development of new prediction tools is that the Canadian Navy is composed predominantly of frigate-type vessels, with lengths of approximately 120 m and displacements of approximately 4500 tonnes; thus, a minimum requirement for new prediction codes is that they must give reliable values for frigate design loads. Clarke [1] gives an overview of wave loading of frigates. Vertical bending moment dominates the structural design. In addition to ultimate strength, fatigue is important for both safety and economic reasons. Horizontal bending moment is generally much less important because of smaller loads and greater strength. For an intact frigate, torsion is usually insignificant; however, torsional loading can become important for a damaged frigate.

Nonlinear effects generally cause the wave-induced sagging moment to be greater than the wave-induced hogging moment. As indicated by Jensen and Pedersen [2], nonlinear effects and resulting sag/hog ratios tend to be greater for finer hull forms. The assumption of linearity implies that the ship sides are vertical at the waterline, which tends to be violated as hull form becomes finer. Modern frigates typically have significant bow flare and wide transom sterns with shallow draft, leading to significant nonlinearities as relative motions increase.

The elastic response of a ship to hydrodynamic loading can significantly influence the resulting bending moments. Jensen and Pedersen [2] and Troesch [3] discuss cases of cargo ships having fundamental structural frequencies in the range of exciting wave encounter frequencies, leading to springing phenomena; however, naval frigates have fundamental structural frequencies which are typically much higher than wave encounter frequencies, causing springing response to be insignificant. For frigates, transient slamming forces of large magnitude and short duration induce whipping loads which can be of major importance in structural design. Clarke [1] indicates that slamming forces can cause up to half the total bending moment at midships; thus, design loads for frigates should include slamming effects. Another important observation for frigates is that whipping forces induced by slamming tend to be greatest during wave-induced sagging and are usually significantly damped during hogging; thus, whipping forces tend to increase the sag/hog ratio for design wave loads.

Belik et al. [4, 5] present time domain simulations for computing ship structural response in waves including slamming effects. They indicate that there are significant uncertainties with predicted hydrodynamic slamming forces.

Due to the limitations of numerical prediction methods, research continues with model tests and full scale trials. Model tests have several advantages relative to full scale trials and numerical simulations. Compared to full scale trials, model tests are usually less expensive and permit greater control and monitoring of environmental conditions. Consequently, model test data are generally more reliable and can be used more confidently for tasks such as validation of prediction software. For examination of ship loads in severe seas, the required conditions can be produced relatively easily for model tests. In contrast, a full scale trial of ship loads in severe seas would entail waiting for sufficiently severe sea conditions, which would then present significant risk to the ship and its crew. Despite great progress in numerical prediction tools for sea loads, model tests are still required for validation, particularly for nonlinear phenomena such as green seas loading and slamming.

Lloyd et al. [6, 7] give a comprehensive data set of motions and sea loads for a rigid warship model in regular oblique waves. The majority of tests have a nominal wave steepness H/λ of $1/50$, giving small amplitude loads and motions which are suitable for

validation of linear frequency domain codes. Hydroelastic models have been successfully tested by several authors, including Troesch [3], Fukasawa et al. [8], Achterides [9], Chou et al. [10], and Dong and Lin [11].

The open literature test data cited above does not include a hydroelastic model of a frigate-type vessel. The Canadian Navy felt that a hydroelastic model test program could provide useful data for both structural design and validation of numerical prediction software. The ship selected for this study was the Canadian Patrol Frigate (CPF), the latest major warship to be introduced into the Canadian fleet. The principal objectives of the project were:

- to determine the magnitude and distribution of wave-induced loads for the CPF in severe seas and to identify the conditions that produce the most severe loads,
- to determine the validity of linear frequency domain codes for modern frigates, characterized by fine hull forms and wide transom sterns,
- to determine the influence of nonlinear effects by using waves of different steepness,
- to determine the magnitude of slam-induced whipping loads.

In 1989, a contract was let to Fleet Technology Limited to undertake a feasibility study to establish the means to meet the above objectives using a hydroelastic model.

FEASIBILITY STUDY

Since the use of physical hydroelastic models for the study of structural responses in model basins was quite novel at the time the project commenced, the first stage was to conduct a feasibility study. This study explored the wave conditions leading to the worst loading cases for the frigate, developed the general model concept, and proposed an experimental program.

Wave Conditions

The wave conditions for the experiments were to represent conditions associated with the extreme ship lifetime value for vertical bending moment at midships. Based on traditional design practice, it was assumed that the design load condition would occur in head seas for a wavelength of the order of the ship length. Model tests on a warship by Lloyd et al. [6, 7] support this assumption, leading to a nominal wave period of 9 seconds in deep water for a wavelength equal to the frigate length of 130 m. The wave height for the design load condition would be determined by limitations on wave steepness, which are discussed in detail by Sarpkaya and Isaacson [12]. The theoretical limit for wave steepness H/λ is 1/7; however, maximum observed wave steepnesses are more commonly in the range 1/15 to 1/10. For wavelengths equal to the length of the frigate, the maximum wave height will be approximately 10 m. Assuming a Rayleigh distribution for wave heights, this maximum wave height will occur once every 3000 wave encounters in an irregular seaway with a significant wave height H_s of 5 m.

Required Model Functions

A key requirement was the establishment of bending moment and shear force distributions along the hull in severe sea conditions. Also of interest was the magnitude of slam-induced whipping loads. The ship model therefore had to:

- model the physical characteristics of the prototype,
- provide measurements of sea loads along its length,
- provide motion measurements in various sea conditions,
- model whipping response.

Elastic Model Design

A literature review provided useful information regarding the elastic model design. As is common for ship hydrodynamic studies, the model had to meet Froude scaling requirements. Lloyd et al. [6, 7] and Lewis [13] used segmented models with Froude scaling to examine wave-induced sea loads; however, their models were essentially rigid and did not model hydroelastic effects. Bishop and Price [14] discuss modelling of elastic properties, which is necessary to include hydroelastic effects. Fukasawa et al. [8] and Achterides [9] give examples of models which successfully match hydroelastic properties.

Two practical model types can achieve the stiffness properties required for a hydroelastic model:

- a PVC model,
- a segmented flexible backbone model.

A segmented model with a continuous flexible backbone was ultimately selected because of its relative

simplicity, cost, and ability to model the required structural properties. Through the use of a continuous backbone, the model comprised a series of segments each exhibiting stiffness and inertial properties of that segment of the hull. A minimum of four segments was required to measure the stresses at midships and the quarter points. To capture the effects of slamming and whipping, a larger number of segments was desired. Compromising between cost and data requirements, it was decided to use six segments along the model length.

Ideally, the flexible backbone would model the stiffness properties of the ship for vertical bending, vertical shear, horizontal bending, horizontal shear, and torsion. Several backbone concepts were designed in steel, aluminum, and composite. Figure 1 shows the composite design that was chosen. By varying the cross-sectional dimensions of the backbone, it would be possible to model the bending and shear stiffness of the ship in both vertical and horizontal directions; however, simultaneous modelling of torsional stiffness and resulting hydroelastic effects would not be feasible.

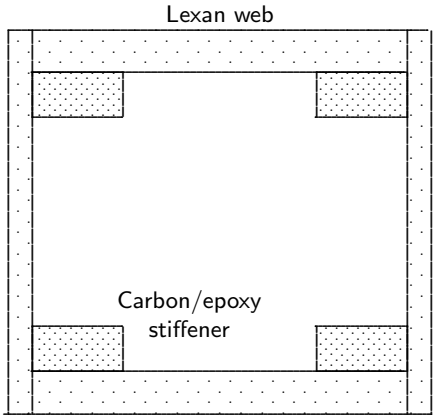

Figure 1: Cross-Section of Composite Model Backbone

Model Testing Facilities

The model test program would require large tank facilities with a capability for generating regular and irregular wave conditions. The Institute for Marine Dynamics (IMD) in St. John's, Newfoundland was selected for all model tests. The Clearwater Towing Tank (200 m long × 12 m wide × 7 m water depth) would be used for tests in head seas, and the Offshore Engineering Basin (75 m long × 32 m wide × 3.5 m depth) would be used for oblique seas tests and a small number of head seas tests to check consistency with towing tank tests.

Model Scale

The model scale was chosen to provide the largest scale model that could be permitted given the physical limitations of the test tanks and the achievable wave heights. The model also had to provide the necessary internal volume for the full range of instrumentation for measurements and vessel control and operation. A final model scale of 1/20 was selected, giving an overall model length of 6.7 m. The relatively small segment sizes would introduce significant challenges for fitting required equipment while matching the prototype weight distribution.

Instrumentation

The model instrumentation would have to provide measurements of all ship motions and sea loads. In addition to rigid body motions, deflections due to elastic deformation were to be obtained. The following shipboard instrumentation was required:

- strain gauge arrays at segment joints to provide vertical and horizontal bending moments, vertical and horizontal shear forces, and torsional moments,
- an inertial reference unit at the vessel CG to provide angular and translational ship motions,
- accelerometers in ship segments to give ship-fixed vertical accelerations measured directly on the backbone,
- a tachometer for propeller RPM,
- an angular displacement transducer for rudder motion.

Test Plan

To fulfill the objectives of the model test program, the feasibility study recommended that experiments proceed in the following order:

- measurements of modal properties of the model using dry and wet hammer tests and shaker tests,
- shakedown tests to isolate responses induced by the propulsion system,
- towed tests in regular and irregular waves, with data acquisition via umbilical cord from the model,

- free-running tests in regular and irregular waves, with data acquisition via telemetry from the model.

MODEL CONSTRUCTION AND OUTFIT

As recommended in the feasibility study, the CPF hydroelastic model was built to a scale of 1/20 using a composite backbone. Table 1 gives the corresponding full scale dimensions for the completed model in fresh water. The body plan is shown in Figure 2 and an overall geometrical layout is shown in Figure 3. The final model design was segmented at stations 2.5, 5 (forward quarter point), 7.5, 10 (midships) and 13.7 (station 0 is FP, 20 is AP). The last segment had to be made rather large to contain all the propulsion and rudder equipment.

Table 1: Full Scale Dimensions for Frigate Hydroelastic Model in Fresh Water, Deep Departure Condition

Length overall, L_{oa}	134.7 m
Length between perpendiculars, L	124.5 m
Beam, B	14.8 m
Midships draft, T	4.97 m
Trim by bow	0.04 m
Displacement, $\triangle$	4655 tonnes
LCG station	10.45
Center of gravity above keel, $\overline{KG}$	6.26 m
Metacentric height, $\overline{GM}$	1.08 m
Roll period in water, T_4	12.3 s

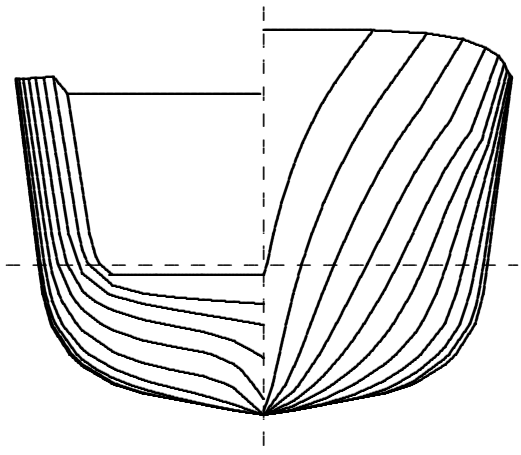

Figure 2: Body Plan for CPF Hydroelastic Model

Hull Construction

The hull consisted of six segments constructed of fibreglass. A foam plug was cut by a numerical milling machine, followed by hand-finishing. A fibreglass mould was next lifted off this plug. The final fibreglass model was then laid up inside this mould, with 10 mm thick bulkheads placed in the appropriate segment locations for segment separation. After placement of the bulkheads, the model was cut into its six segments.

Backbone Construction

Figure 1 shows a cross-section of the model backbone, which consisted of a longitudinal box made of polycarbonate Lexan, with a longitudinal carbon/epoxy stiffener at each corner. The stiffeners were attached to the box using screws and glue. At six longitudinal locations inside the backbone, corresponding to the hull segment mounting platforms, solid hardwood bulkheads were fitted. Neither the wooden bulkheads nor the Lexan webs were longitudinally continuous; thus, the carbon fibre stiffeners were the only longitudinal structural members spanning the whole model. The backbone was centered transversely in the model and the vertical height of its centerline coincided with the model vertical neutral axis at midships, which was 5.40 meters (full scale) above the keel.

The backbone was designed and built to model the stiffness properties of the CPF for vertical bending, vertical shear, horizontal bending, and horizontal shear. For Froude scaling of stiffness properties, the bending rigidity EI^A scales as λ^5 and the shear rigidity GA^S scales as λ^3, where E is elastic modulus of material, I^A is second moment of structural cross-sectional area, λ is length scale factor, G is shear modulus of material, and A^S is cross-sectional shear area. For the model backbone section of Figure 1, the carbon epoxy stiffeners (E = 152 GPa) provide the bending stiffness and the Lexan web (G = 0.78 GPa) provides the shear stiffness. Table 2 gives the full scale sectional stiffnesses of the CPF at the model segment joints.

The cross-sectional height of the backbone is 127 mm, and the height of each of the four stiffeners is 10 mm. Other cross-sectional dimensions of the backbone vary continuously along its length such that the stiffness properties are correctly modelled at the five segment joints. The procedure for determining the remaining cross-sectional backbone dimensions at each segment joint was as follows:

- determine carbon/epoxy girder width to match

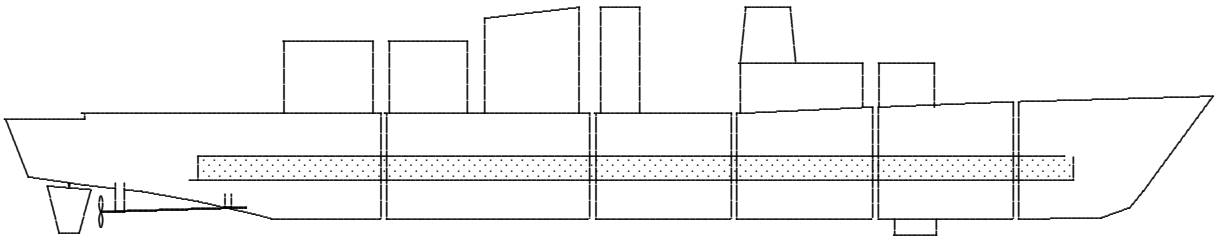

Figure 3: CPF Hydroelastic Model Profile

Table 2: CPF Full Scale Stiffness Properties at Segment Joints

Station	Stiffness			
	Vertical Bending EI^A_{yy} (GN·m^2)	Horizontal Bending EI^A_{zz} (GN·m^2)	Vertical Shear GA^S_v (GN)	Horizontal Shear GA^S_h (GN)
2.5	1364	1459	10.4	16.0
5.0	1799	2316	9.4	20.9
7.5	2080	3455	9.3	19.4
10.0	2521	4486	9.4	23.0
13.7	2151	3600	8.9	23.5

vertical bending stiffness (range of 18.9 to 35.0 mm),

- determine horizontal girder spacing to match horizontal bending stiffness (range of 103 to 133 mm),
- determine thickness of vertical walls to match vertical shear stiffness, (range of 7.1 to 8.3 mm)
- determine thickness of horizontal walls to match horizontal shear stiffness (range of 12.0 to 14.7 mm).

Fitting of Hull Segments to Backbone

For attaching the backbone to the hull, each hull segment was fitted with an aluminum mounting platform with a hardwood mounting surface. The six model segments were placed in the hull mold and the mounting surfaces were machined to the same horizontal level to ensured perfect seating of the backbone, which was then bolted to the model segments. A horizontal gap of 10 mm separated the model segments so that the adjacent segments would not touch each other as the model flexed and twisted during wave tank tests. The gaps were sealed with thin latex strips cemented to the hull surface. These strips were strong enough to withstand elastic stretching and twisting, but thin and flexible enough not to absorb any appreciable loading on their own.

Deck and Superstructure

A simplified deck and superstructure were built, including the forward deck breakwater, so that the presence of green water on deck could be modelled. The deck and superstructure were made of Lexan and Plexiglas, and were cut at each segment joint to break longitudinal continuity.

Appendages

The CPF is a twin-screw, single rudder design and is fitted with bilge keels and a single centerline sonar dome. The propeller shaft brackets were machined out of aluminum. The bilge keels were constructed using stainless steel sheets and were cut at the hull segment joints to break longitudinal continuity. The sonar dome and the rudder were made of hardwood. The rudder was actively controlled by a servo motor, which was operated by remote-control.

Propulsion System

The model was fitted with a pair of 4-bladed inward-turning stock propellers, with full scale diameters of 3.66 m. Due to the large size of the model backbone, the design of the propulsion system was largely driven by space constraints. Two separate motors were fitted to drive the propellers. The motors were directly connected to the propellers via the

propeller shafts, with no reduction gear boxes. The propeller speed was operated by remote-control.

Final Ballasting

Power was supplied by a set of heavy duty deep cycle batteries installed in the various segments but connected together to form a power network. These batteries formed a high proportion of the ballast in the model and therefore their location was dictated by the ballast distribution requirements. Most experiments were conducted for the CPF in the deep departure condition, with additional experiments for the operational light condition. All data in this paper are for the deep departure condition unless noted otherwise. The model segments were ballasted to match the inertial properties of the CPF, with Table 3 giving the achieved values. Figure 4 gives the estimated sectional mass distribution which was used for subsequent numerical predictions of ship motions and sea loads in waves.

Table 3: Model Segment Inertial Properties

Segment	Stations	Mass (tonnes)	LCG (station)	$\overline{KG}$ (m)
1	0.0-2.5	180	1.12	7.20
2	2.5-5.0	507	3.73	6.45
3	5.0-7.5	672	6.32	6.93
4	7.5-10.0	801	8.70	6.05
5	10.0-13.7	1155	11.72	5.99
6	13.7-20.0	1340	16.28	6.08
Ship	0.0-20.0	4655	10.45	6.26

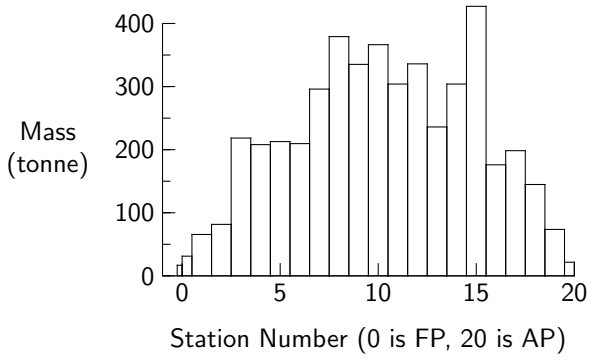

Figure 4: Sectional Mass Distribution

Natural Bending Frequencies

After final ballasting, measurements were made of the natural vertical bending frequencies of the hydroelastic model in water and air. Table 4 gives the measured vertical bending frequencies in water and values for the full scale ship computed by a finite element program. For vertical bending frequencies, the model gives excellent agreement for the first and third modes but has a significantly lower natural frequency for the second mode. Although the model was constructed to match the horizontal stiffness properties of the ship, no measurements were taken of the model natural frequencies for horizontal bending. The horizontal bending frequencies of the model likely achieved accuracies similar to those for vertical bending.

Table 4: Full Scale Natural Bending Frequencies for CPF in Water

Mode	Natural frequency (Hz)	
	Model (measured)	Ship (computed)
1st vertical	1.42	1.44
2nd vertical	2.69	3.14
3rd vertical	4.48	4.57
1st horizontal		1.82
2nd horizontal		3.95
3rd horizontal		4.72

In addition to the three vertical bending modes given in Table 4, the CPF hydroelastic model had an additional mode with a full scale wet natural frequency of 1.00 Hz. This mode was due to cantilevering of the aft model segment at the segment joint, and was caused by the relatively long segment length and large segment mass.

Table 5 gives measured damping coefficients for the vertical bending modes of the CPF hydroelastic model in air and water. The damping values are nondimensionalized by critical damping, with the critical damping values for water including added mass effects for each mode. The measured damping coefficients suggest that there is some hydrodynamic damping for the first bending mode but negligible hydrodynamic damping for the second and third modes. The vertical bending modes have natural frequencies above the range of significant wave radiation damping. Although no attempt was made to model the structural damping characteristics of the CPF, the measured damping coefficients are remarkably close to values of approximately 3 percent

given by Bishop et al. [15] for the first three vertical bending modes of a full scale frigate.

Table 5: Vertical Bending Damping Coefficients for CPF Hydroelastic Model

Mode	Damping ratio (percent)	
	Dry	Wet
1st vertical	2.3	2.7
2nd vertical	2.5	2.5
3rd vertical	3.1	3.1

As mentioned previously, no attempt was made to model the torsional stiffness properties of the CPF; however, calculations based on the model properties indicate that the first torsional mode has a full scale natural frequency of approximately 4 Hz, similar to the predicted value for the prototype ship. This frequency is much higher than expected wave encounter frequencies, suggesting that hydroelastic effects will be negligible for torsion.

INSTRUMENTATION

Extensive instrumentation provided measurements as recommended in the feasibility study.

To measure sea loads, the backbone was instrumented with strain gauge bridges at each of the five segment joints. The strain gauge bridges provided measurements of vertical bending, vertical shear, horizontal bending, horizontal shear, and torsion. Before attaching the ship hull segments to the model backbone, an extensive calibration was performed to determine relationships between applied loads and measured strains on the backbone. The calibration was performed by applying a series of known loads to the backbone. It was assumed that strains were linear and that strains at a given longitudinal segment joint were not affected by strains at another longitudinal segment joint. Due to imperfections in the backbone properties, some "cross-talk" effects exist and are included in the calibration. For example, a pure vertical load will cause a measured torsional strain. The calibration process produced a 5×5 matrix for each segment joint relating measured strains to loads.

To measure whipping acceleration for each hull segment, accelerometers were rigidly mounted on top of the backbone at stations 1.93, 3.69, 6.18, 8.67, 11.73 and 16.71. These accelerometers required a frequency response extending to 25 Hz (model scale) so that accurate measurements could be made up to the third vertical mode of backbone vibration.

In addition to the backbone instrumentation, a stable platform (also called "inertial reference unit") was fitted at the model center of gravity to measure the global motions (linear accelerations and angular displacements). Linear model displacements were later derived from the acceleration data. A capacitance wave probe was mounted at the forward perpendicular (weather side) to measure the relative motion between the model and the wave surface. Port and starboard propeller speeds and rudder angle were also measured as aids to data analysis and for quality control. During wave tank tests, wave elevation was measured using standard capacitance wave probes.

Two separate data acquisition systems and rates were employed. An onboard computer was used to sample backbone data at a frequency of 200 Hz (model scale), which was sufficiently high for whipping responses. Data for global model motions, relative motion, propeller speed, and rudder angle were filtered at 10 Hz and telemetered to a shore-based computer.

EXPERIMENTAL PROGRAM

The experimental program included tests in regular and irregular wave conditions. Additional tests in calm water provided measurements of vertical shear force and bending moment due to ship forward speed.

The rudder angle and propeller rate were radio controlled by a human operator. Desired test speeds in waves were achieved by setting the mean propeller revolutions to those obtained from prior calibration and were checked by manually measuring the time needed to travel a known distance. The actual model speed for all tests was within five percent of the target speed. Tests in oblique seas were conducted in a model basin. Head seas tests were conducted in the towing tank, with some additional tests in the model basin to verify consistency between facilities. The model was free-running for all towing tank and model basin tests presented in this paper.

Table 6 gives conditions for regular wave tests for the deep departure loading condition. Some additional tests in regular head seas were performed for the operational light loading condition. Table 7 gives conditions for irregular waves tests using Bretschneider spectra. A heading of 180 degrees corresponds to head seas; thus, all tests were conducted in head and bow quartering seas.

Table 6: Regular Wave Tests

Heading (degrees)	Froude Number	Wave Steepnesses
180	0.06	1/30, 1/20, 1/15
	0.12	1/30, 1/20, 1/15
	0.20	1/30, 1/20
	0.25	1/30
165	0.06	1/30, 1/20
	0.12	1/30, 1/20
	0.20	1/30, 1/20
	0.25	1/30
135	0.12	1/30, 1/20
	0.20	1/30, 1/20
	0.25	1/30

Table 7: Irregular Wave Tests

Heading (degrees)	Froude number	H_s/T_p pairs
180	0.06	4 m/9 s, 5 m/11 s, 6 m/13 s
	0.12	4 m/9 s, 5 m/11 s, 6 m/13 s
	0.20	4 m/9 s, 5 m/11 s, 6 m/13 s
	0.25	4 m/9 s, 5 m/11 s, 6 m/13 s
165	0.06	5 m/11 s
	0.12	5 m/11 s
	0.20	5 m/11 s
150	0.06	5 m/11 s
	0.12	5 m/11 s
	0.20	5 m/11 s
135	0.06	5 m/11 s
	0.12	5 m/11 s
	0.20	5 m/11 s

FREQUENCY DOMAIN PREDICTIONS OF MOTIONS AND LOADS

The strip theory program SHIPMO and the three-dimensional program PRECAL provided frequency domain predictions of motions and sea loads for the CPF hydroelastic model. SHIPMO and PRECAL are the two main computational tools currently being used by the Canadian Navy for predicting ship motions and sea loads. Ongoing research is examining more sophisticated computational methods which include nonlinear effects.

Strip Theory Code SHIPMO

McTaggart [16] gives a detailed description of the most recent version of SHIPMO, which is based largely upon the theory of Salvesen, Tuck and Faltinsen [17]. Schmitke [18] demonstrated that appendage and viscous forces significantly influence lateral plane motions, and implemented these forces into SHIPMO. Although SHIPMO is essentially a linear code, it uses an iterative procedure to obtain the roll amplitude and effective linearized damping for the prescribed sea conditions.

Recent development efforts have aimed to produce an accurate and robust tool for predicting sea loads. To achieve maximum accuracy for sea load predictions, all forces influencing ship motions and sea loads must be considered in a consistent manner. SHIPMO lateral plane load predictions include the appendage and viscous forces which are used for motion predictions. Careful numerical integration ensures consistency of forces acting along the length of the ship for motion and load predictions.

Irregular frequencies and low encounter frequencies can cause severe errors for strip theory predictions. The latest version of SHIPMO uses a boundary element method from Sclavounos and Lee [19] to eliminate irregular frequencies. To avoid problems at low encounter frequencies, all motion and load computations are performed at wave frequencies with encounter frequencies greater than $0.5\sqrt{g/L}$. If a wave frequency has an encounter frequency below this threshold, motions and sea loads are estimated by interpolation of results from other wave frequencies.

The warship model of Lloyd et al. [6, 7] was used to validate motion and sea loads predictions during code development. Figure 5 shows the waterplanes of the warship and the CPF. While the CPF has a transom stern, the warship has a narrow stern which is more consistent with the assumptions of strip theory; thus, the warship model data were more suit-

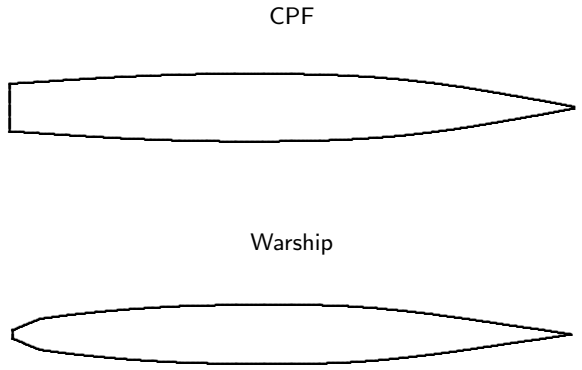

Figure 5: Waterplanes for CPF and Warship of Lloyd et al.

able for assessing if SHIPMO correctly implemented strip theory. Figure 6 illustrates the good agreement between SHIPMO and the warship experiments for vertical bending at midships.

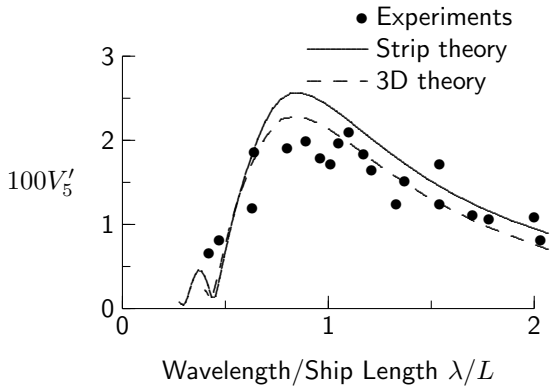

Figure 6: Vertical Bending Moment at Midships in Regular Head Seas for Warship at $Fn = 0.21$

A critical test for sea load predictions is that all loads must be zero at either end of the ship. In SHIPMO, sea loads are obtained through integration of forces forward of the station in question; thus, non-zero computed sea loads at the aft end of the ship will reveal any inconsistencies between forces used for ship motions and sea loads. SHIPMO gives successful closure for all load modes. McTaggart [16] gives additional validation results for the warship model, indicating excellent agreement for motions and good agreement for sea loads.

Preparation of SHIPMO input was relatively easy using the known dimensions for the CPF hydroelastic model. Input sectional masses were based on estimates from properties of all model components. The sectional vertical center of gravity locations were based on measured vertical center of gravity locations for the six model segments. Using the vertical center of gravity heights given in Table 3, the computed metacentric height was 1.32 m, compared to the measured value of 1.08 m. To obtain agreement between computed and measured metacentric heights, ship and sectional centers of gravity used in all motion and load computations were raised by 0.24 m (3.8 percent of the reported ship $\overline{KG}$ value). With respect to roll inertia, the only known property for the CPF hydroelastic model was its measured roll natural period of 12.3 s (deep departure condition, full scale). Using this value and the roll added mass predicted by SHIPMO, the full scale dry roll gyradius of the model was assumed to be 5.82 m. The sectional roll gyradii were estimated by assuming the following relationship, which assumes that the mass along each section is represented by a circular cylinder with uniform density:

$$r_{xx-i} = k_r \sqrt{\frac{m_i}{l_i}} \quad (1)$$

where r_{xx-i} is the sectional roll gyradius about the sectional center of gravity, k_r is a proportionality constant valid for all sections, m_i is sectional mass, and l_i is sectional length. The proportionality constant k_r was determined by satisfying the estimated dry roll gyradius of 5.82 m.

A wave steepness of 1/30 was used for predicting roll damping and resulting lateral plane motions and sea loads in regular waves. Although the experiments included wave steepnesses of 1/20 and 1/15, SHIPMO predictions showed little variation with wave steepness for the speeds and headings considered in the present study.

Three-Dimensional Code PRECAL

The three-dimensional code PRECAL has been developed by Cooperative Research Ships, which consists of member organizations who jointly fund and perform research projects related to ship design. PRECAL, which has been under development since 1984, predicts ship motions, sea loads, and hydrodynamic pressures acting on a ship in waves.

The theoretical basis of PRECAL is similar to three-dimensional codes developed by Chang [20] and Kim et al. [21]. Wehausen and Laitone [22] give equations for Green functions at zero forward speed and non-zero speed which are used for solving the flow field around the ship. At forward speed, PRECAL can use the forward speed Green function or approximations based on the zero speed Green function. The theoretical formulation for using the zero

speed Green function at forward speed assumes high wave encounter frequency, low forward speed, and a slender hull form. In practice, the forward speed Green function is rarely used by PRECAL users because of high computational requirements and numerical instabilities; thus, all computations in this paper use the zero speed Green function.

Roll damping predictions from SHIPMO were considered to be more reliable than those from the version of PRECAL used in the present study; thus, SHIPMO roll damping coefficients were used as input to PRECAL. For the range of experimental conditions included in the test program, the SHIPMO roll damping coefficients indicated that nondimensional roll damping (taken as a fraction of critical damping) showed little variation with wave frequency. The PRECAL roll computations for a Froude number of 0.12 and regular seas with a heading of 135 degrees use a roll damping coefficient of 0.147, which was computed by SHIPMO for a wave steepness of 1/30 and a wave frequency having an encounter frequency corresponding to the natural roll frequency of the model. For a Froude number of 0.12 and irregular seas with a heading of 135 degrees, significant wave height of 5 m, and peak wave period of 11 s, a roll damping coefficient of 0.093 was obtained from SHIPMO for a wave encounter frequency equal to the natural ship roll frequency.

The dry sectional roll gyradii for PRECAL were taken as being equal to the estimated values for SHIPMO. Due to differences between PRECAL and SHIPMO roll added masses, the roll natural period determined by PRECAL was 11.8 seconds, which is 4 percent lower than the measured value of 12.3 seconds.

OSCILLATORY WAVE-INDUCED MOTIONS AND SEA LOADS

This section gives selected experimental results and frequency domain predictions of oscillatory wave-induced motions and sea loads. For loads in regular waves, shear forces at station 5 and bending moments at midships (station 10) are presented. Loads are given at the five model segment joints for irregular seas.

For regular seas, motions and sea loads are given as nondimensional amplitudes as follows:

$$\zeta_i' = \frac{\zeta_i}{a} \text{ for } i = 1-3 \quad (2)$$

$$\zeta_i' = \frac{\zeta_i}{ka} \text{ for } i = 4-6 \quad (3)$$

$$V_i' = \frac{V_i}{\rho g L B a} \text{ for } i = 1-3 \quad (4)$$

$$V_i' = \frac{V_i}{\rho g L^2 B a} \text{ for } i = 4-6 \quad (5)$$

where ζ_i' is nondimensional motion amplitude, ζ_i is dimensional motion amplitude, a is wave amplitude, k is wavenumber, V_i' is nondimensional load amplitude, and V_i is dimensional load amplitude. For motions, the order of modes corresponding to subscript i is surge, sway, heave, roll, pitch, and yaw. For loads, the order of modes is axial, horizontal shear, vertical shear, torsion, vertical bending, and horizontal bending.

Figure 7 shows vertical plane responses in regular head seas and Figure 8 shows lateral plane responses in regular oblique seas. The amplitude for each motion and load component is taken as $\sqrt{2m_0}$, where m_0 is the area under the response spectrum. The spectral area m_0 is calculated for a relatively narrow frequency range in the vicinity of the wave encounter frequency for each model test; thus, the regular seas amplitudes do not include effects such as whipping, which occur at frequencies significantly higher than the experimental wave encounter frequencies.

Figure 9 shows motions in irregular seas and Figure 10 shows load distributions. Motions and sea loads are given as full scale RMS values. The RMS value for each motion and load component is $\sqrt{m_0}$, where m_0 is the spectral area across the entire range of encounter frequencies having significant wave spectral energy.

The experimental regular seas data in Figures 7 and 8 show that nondimensional motions have little variation with wave steepness, while nondimensional sea loads tend to decrease slightly as wave steepness increases. The high degree of consistency of the regular seas data supports the validity of the data. The experimental data for irregular seas in Figures 9 and 10 also appear to be consistent, with the exceptions of yaw at Froude number 0.12 and torsion at station 13.7.

The comparisons between experimental results and frequency domain predictions show generally good agreement, with motion predictions being better than sea load predictions and three-dimensional predictions being better than strip theory predictions. Strip theory consistently overpredicts sea loads, although the degree of overprediction appears acceptable in most cases. Numerical roll predictions are greater than experimental values. For torsion, the strip theory predictions are much higher than the experimental values while the three-dimensional code gives moderate overpredictions.

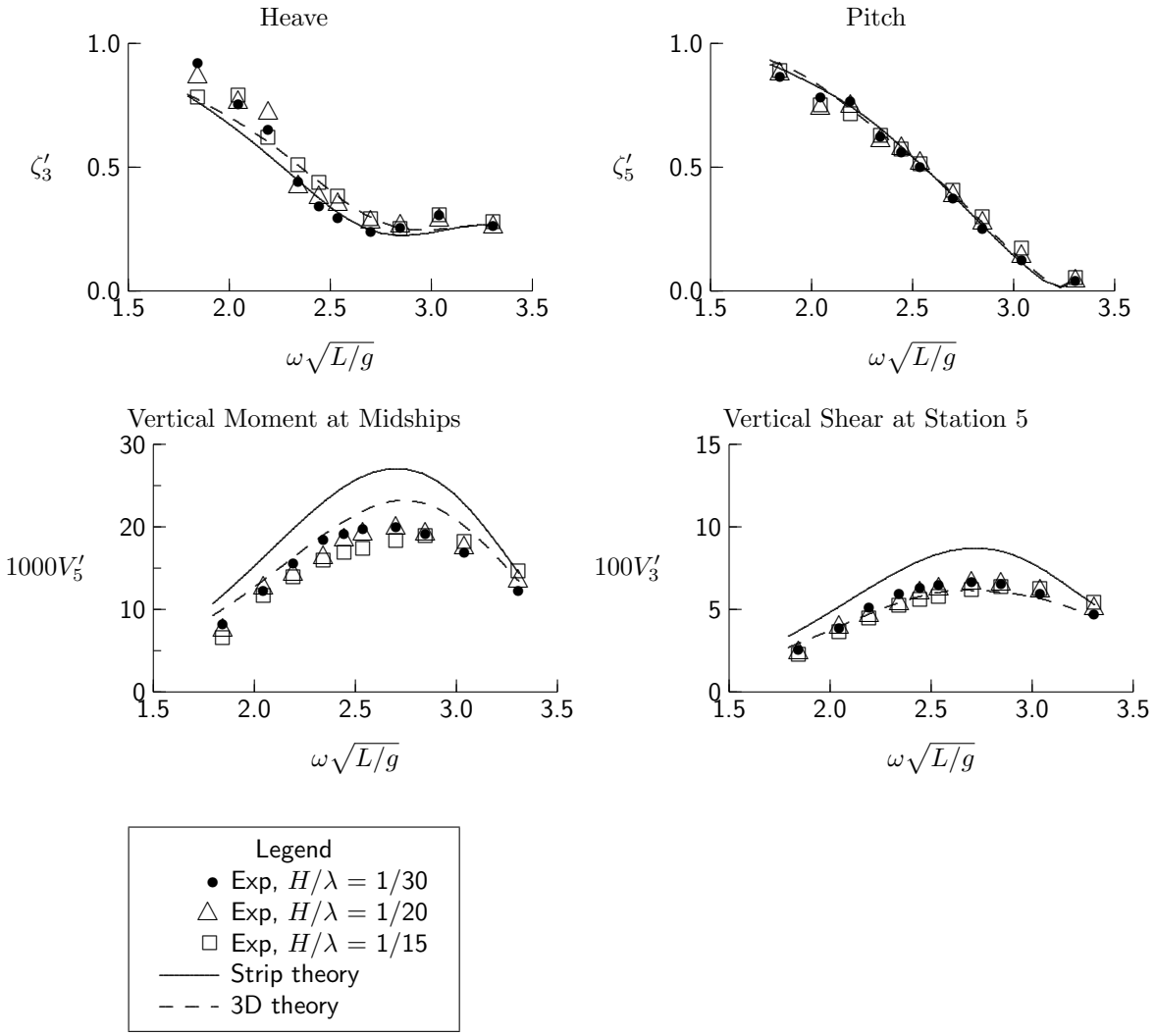

Figure 7: Vertical Plane Responses in Regular Waves, Head Seas, $Fn = 0.12$

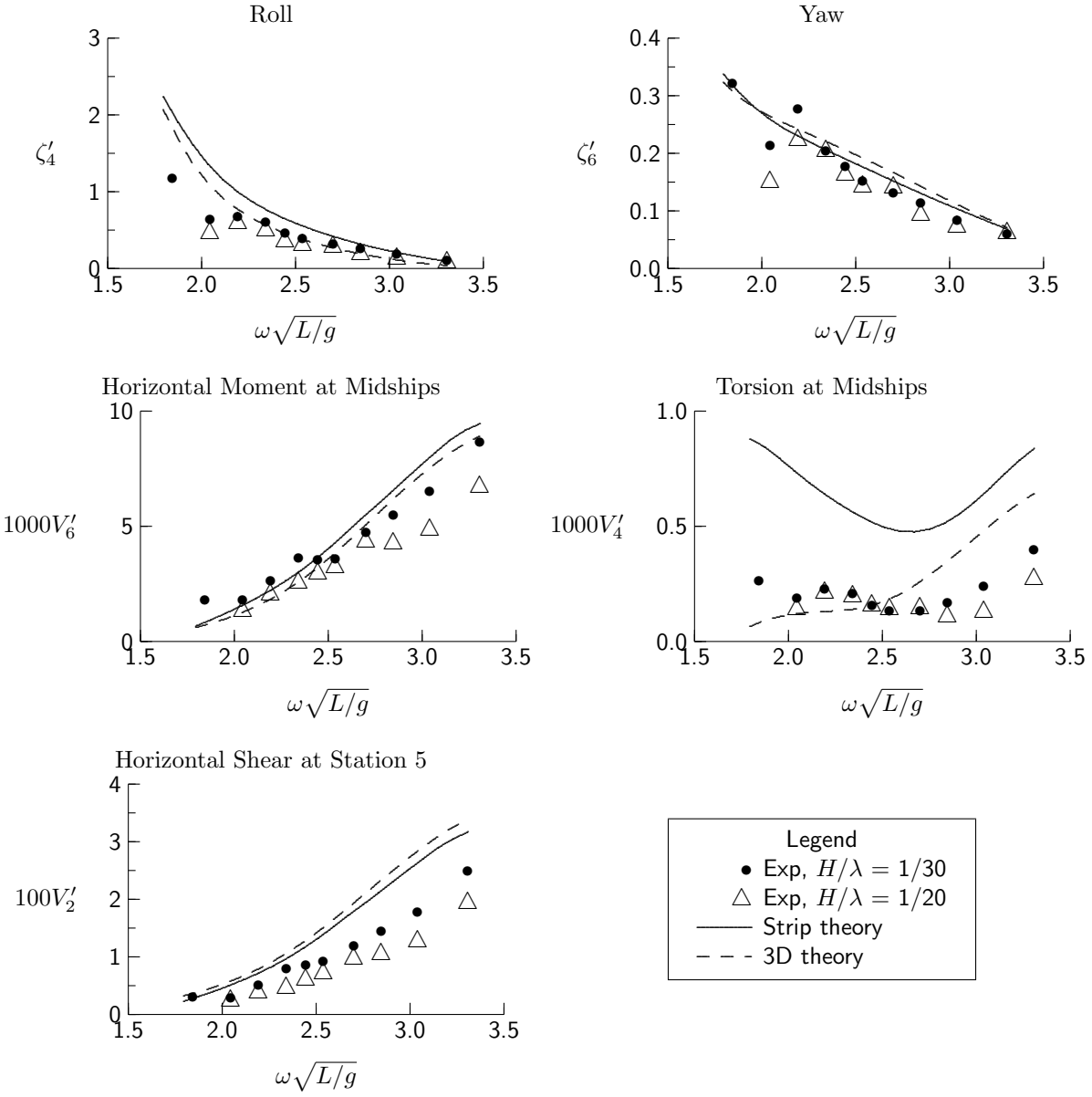

Figure 8: Lateral Plane Responses in Regular Waves, Oblique Seas, $\beta_s = 135$ degrees, $Fn = 0.12$

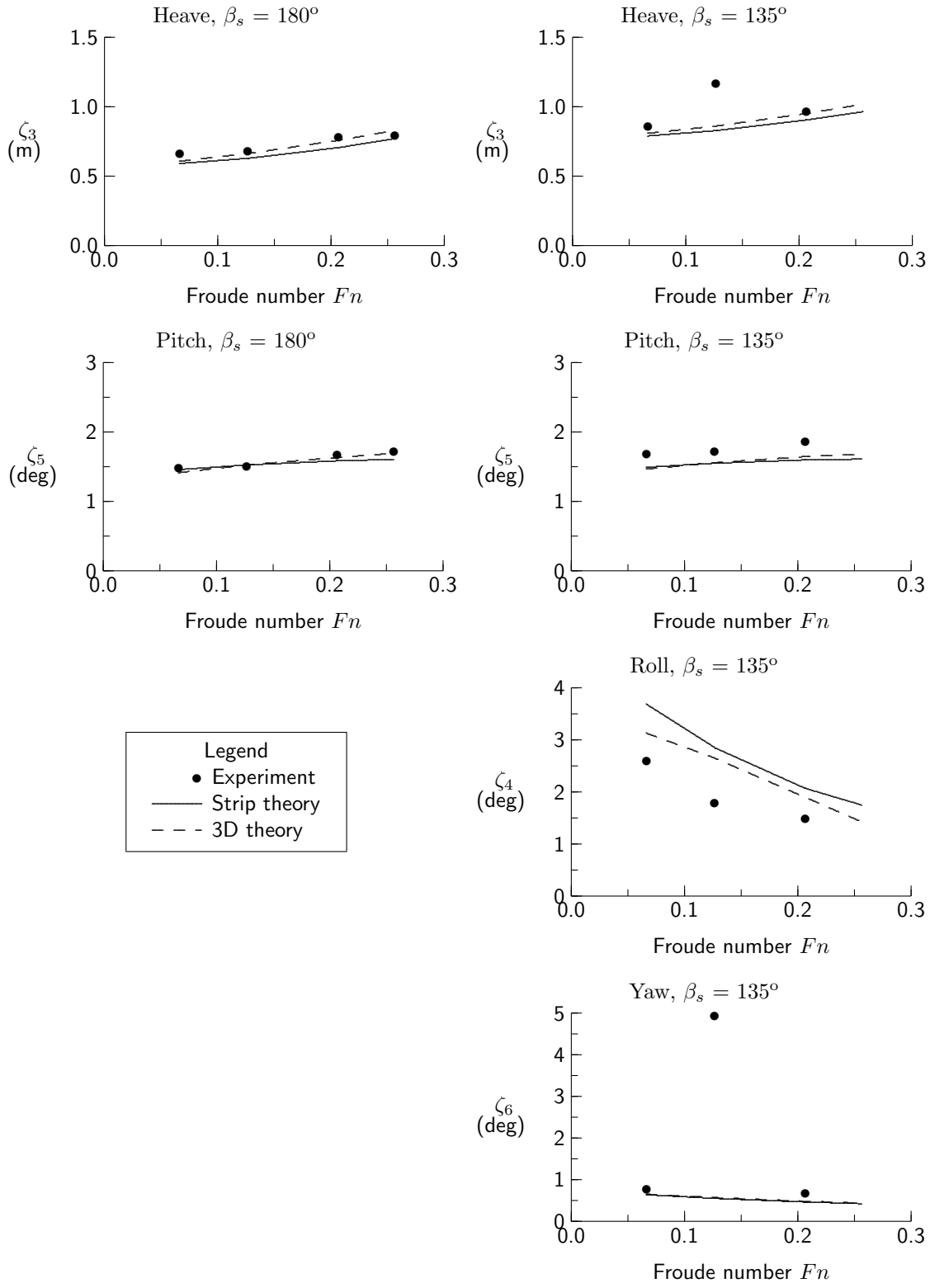

Figure 9: RMS Motions in Irregular Waves, $H_s = 5$ m, $T_p = 11$ s

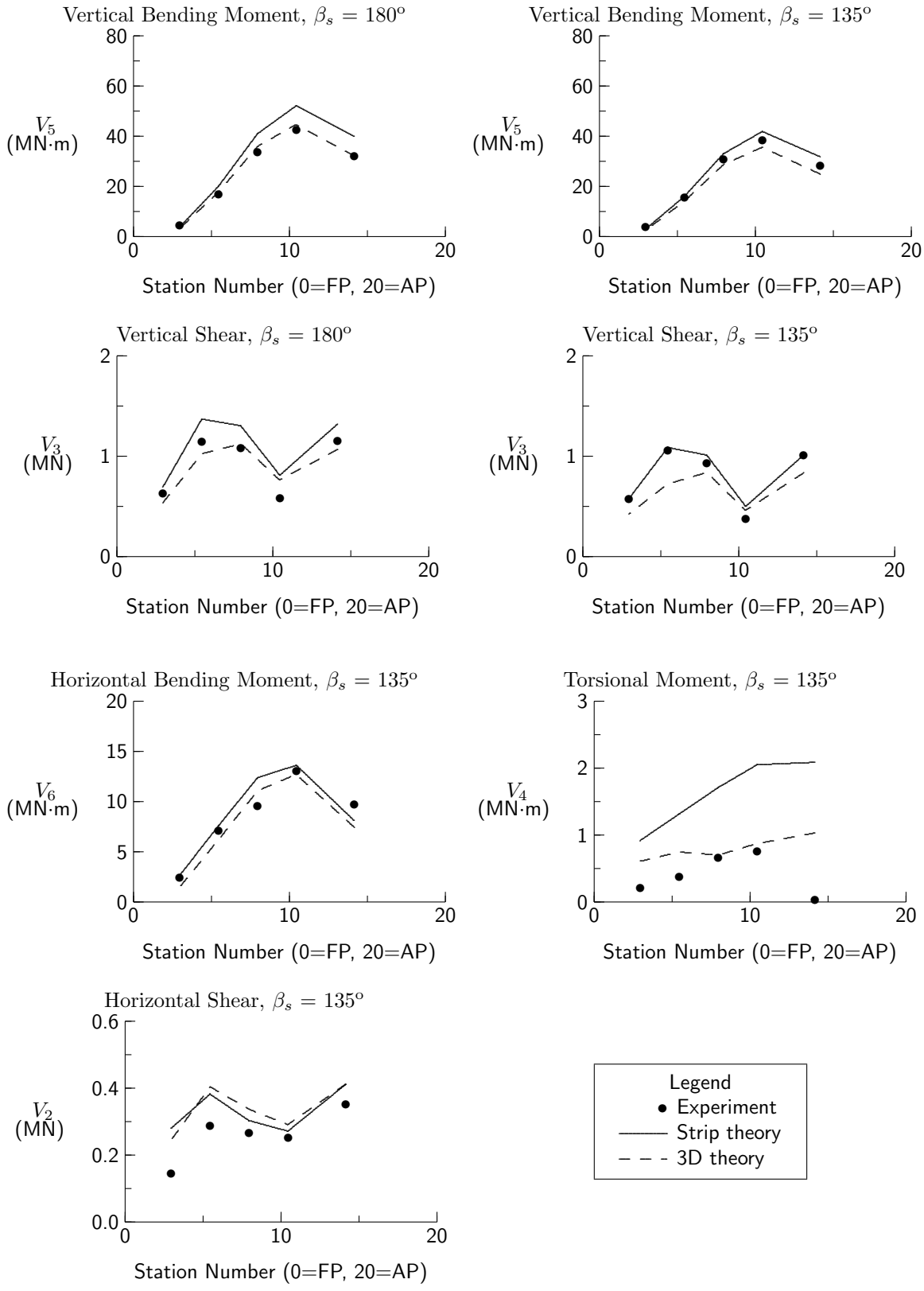

Figure 10: RMS Sea Loads in Irregular Waves, $H_s = 5$ m, $T_p = 11$ s, $Fn = 0.12$

Sources of Discrepancies between Prediction and Experiment

The discrepancies between predictions and experiments arise from several sources. The wide transom stern of the CPF violates the slenderness assumptions of strip theory, and likely causes overprediction of hydrodynamic forces at the ends of the ship and resulting sea loads such as vertical bending moment. Comparison of bending moment predictions in Figures 6 and 7 indicates that strip theory gives better predictions for the narrow stern warship hull of Lloyd et al. than for the CPF. Similar results were observed throughout comparisons of strip theory predictions with data for the CPF and warship. As mentioned previously, the three-dimensional predictions use a zero speed Green function and approximations based on slenderness assumptions; thus, the wide stern also affects the three-dimensional predictions at non-zero forward speed.

The most notable differences between predictions and experimental data occur for torsion in regular waves. These differences become greatest at lower wave frequencies, at which the wave encounter frequency approaches the ship roll natural frequency. Near roll resonance, predicted roll motions and torsional loads can be significantly affected by small errors in hydrodynamic forces. A likely source of error for torsional moment predictions is that the sectional distribution of roll inertia was estimated using Equation (1). The discrepancy between computed and measured metacentric heights mentioned previously suggests possible errors in the segment vertical center of gravity locations given in Table 3.

A major source of differences between the present torsion predictions is that the three-dimensional code incorrectly assumes constant metacentric height along the model length while the strip theory code considers the longitudinal variation of sectional metacentric heights. For the frigate model, the metacentric height of the forward half is much less than the metacentric height of the aft half, which will cause roll displacement to induce large torsional moment at midships; thus, the relatively good agreement of the three-dimensional predictions with experimental results in Figure 8 is surprising and more likely due to chance than to correct modelling of all force components. In contrast, comparisons with the warship data of Lloyd et al. (e.g. Figure 11) indicated that strip theory predictions were much better than three-dimensional predictions. It is postulated that the the poor strip theory predictions of torsion in Figure 8 at lower wave frequencies are due to overprediction of roll motions and resulting restoring moments. At higher wave frequencies, inertial forces become dominant and numerical predictions are likely affected by incorrect roll inertia properties.

The numerical predictions do not include effects of rudder motions, which were human controlled; however, good agreement between measured and predicted yaw motions suggests that the influence of rudder motions was minor. The experimental data show greater scatter for oblique seas than for head seas, which could be caused by variations in rudder motions.

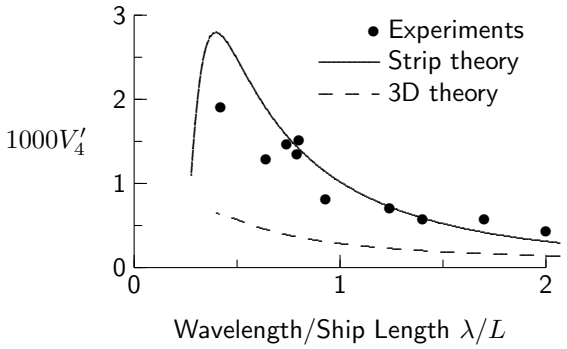

Figure 11: Midships Torsion in Regular Seas for Warship at $Fn = 0.21$, $\beta = 60$ degrees

The experimental results indicate that nonlinear effects have relatively little influence on oscillatory wave-induced motions and loads for the frigate; thus, the limitations of linearity likely have little influence on the accuracy of frequency domain predictions for the frigate experimental conditions.

Further Examination of Wave-Induced Vertical Bending Moment in Irregular Seas

Because of its importance in structural design, additional results and analysis are given for RMS wave-induced vertical bending moment in irregular seas. Figure 12 shows the variation of midships vertical bending moment with ship speed. Over the range of tested ship speeds, the measured wave-induced moment increases by approximately 20 percent as ship speed increases. The results in Figure 12 do not include slamming forces, which will also increase with ship speed. Strip theory consistently overpredicts bending moment by approximately 25 percent. The three-dimensional predictions using the zero speed Green function give excellent agreement at low speed but become approximately 15 percent greater than experimental values as Froude number increases to 0.25.

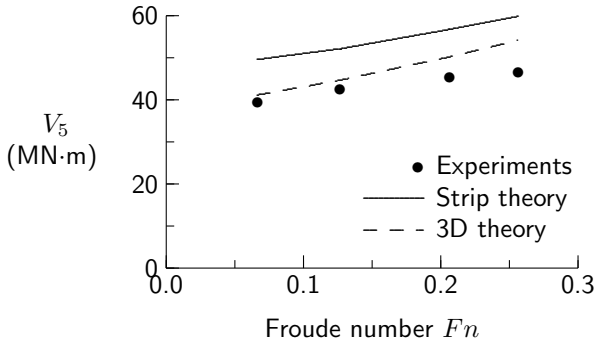

Figure 12: RMS Vertical Bending Moment at Midships Versus Froude Number in Irregular Head Seas, $H_s = 5$ m, $T_p = 11$ s

Figure 13 shows that measured bending moment is greatest for head seas and is slightly smaller for the oblique headings. The numerical predictions maintain good accuracy among the different headings.

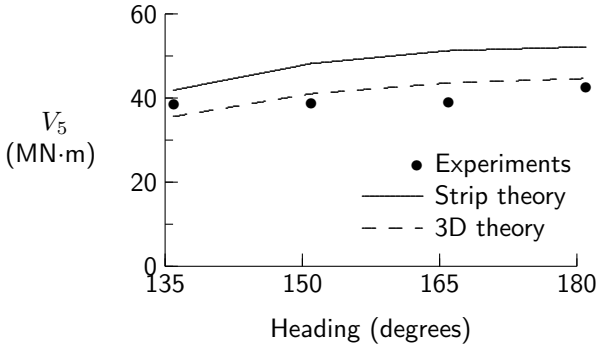

Figure 13: RMS Vertical Bending Moment at Midships Versus Heading in Irregular Seas, $H_s = 5$ m, $T_p = 11$ s, $Fn = 0.12$

The variation of bending moment with significant wave height is given in Figure 14. For the significant wave heights of 4, 5, and 6 m, the associated peak wave periods are 9, 11, and 13 s, as given in Table 7. Vertical bending increases with significant wave height, although the influence of wave period causes this increase to be less than linear. The degree of overprediction by the linear programs increases slightly as wave height increases.

The sensitivity of wave loads to ship loading condition is of great importance to designers. If wave loads are relatively insensitive to ship loading condition, then wave loads for a single loading condition can be considered representative of loads for all loading conditions. Figure 15 shows vertical bending moment distributions for the deep departure condi-

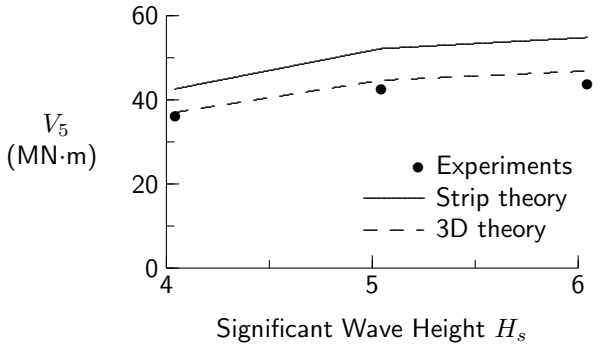

Figure 14: RMS Vertical Bending Moment at Midships Versus Significant Wave Height in Irregular Head Seas, $Fn = 0.12$

tion (fresh water displacement 4655 tonnes) and operational light condition (4191 tonnes). The bending moment distributions calculated from measured RAOs in regular seas show little variation with loading condition. Furthermore, the bending moment distribution calculated from regular seas RAOs for the deep departure condition is almost identical to the measured distribution in irregular waves, indicating the validity of linear superposition.

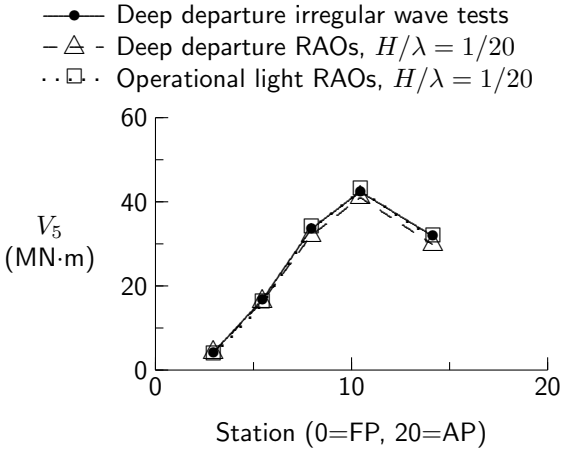

Figure 15: RMS Vertical Bending Moment Distribution in Irregular Head Seas for Deep Departure and Operational Light Conditions, $H_s = 5$ m, $T_p = 11$ s, $Fn = 0.12$

Considering the results presented for wave-induced vertical bending moment, some general comments can be made regarding the accuracy of numerical predictions for the CPF. Strip theory consistently overpredicts vertical bending at midships. This overprediction is likely caused by the non-slender geometry of the CPF, particularly at

the stern. In contrast, the three-dimensional linear theory using the zero speed Green function gives excellent results at low speed. At higher speed, the forward speed Green function could likely give similarly good results. The experimental data and numerical predictions suggest that nonlinear effects are relatively small and that linear frequency domain methods can provide good predictions of oscillatory wave-induced bending moments in most conditions.

MEAN VERTICAL BENDING MOMENTS

In addition to the oscillatory wave loads discussed in the previous section, experimental measurements of mean vertical bending moment were taken in regular waves. The magnitudes of hogging and sagging bending moments acting on a section experiencing oscillatory moments of magnitude V_5 can be expressed as:

$$V_5^{hog} = V_5 - \overline{V}_5^S - \overline{V}_5^U - \overline{V}_5^W \quad (6)$$

$$V_5^{sag} = V_5 + \overline{V}_5^S + \overline{V}_5^U + \overline{V}_5^W \quad (7)$$

where $\overline{V}_5^S$ is the mean still-water bending moment due to the ship mass and buoyancy distribution, $\overline{V}_5^U$ is the mean bending moment due to ship forward speed in calm water, and $\overline{V}_5^W$ is the mean bending moment due to the seaway. The above equations use a sign convention of positive for sagging moments and do not include slamming forces.

Figure 16 shows mean measured bending moment in calm water due to ship forward speed. This bending moment is the difference between bending moment measured at speed and at zero speed in calm water. There was significant scatter in data among different runs for a given ship speed, with the plotted results giving mean values among runs. As expected, the magnitude of the measured bending moment increases with ship speed. The relative importance of mean bending moment due to forward speed can be examined by comparing it with wave-induced bending values such as those given in Figure 12. It is assumed that the maximum bending moment in an irregular seaway will be approximately four times the RMS value. For a Froude number of 0.25, the experimental results of Figure 12 indicate a maximum wave-induced bending moment of approximately 190 MN·m for a ship in head seas with significant wave height of 5 m, compared to a mean value of 8 MN·m due to ship forward speed; thus, mean bending due to ship forward speed is relatively small for the CPF.

Figure 17 gives mean sag moment due to waves at midships in regular head seas at a Froude number

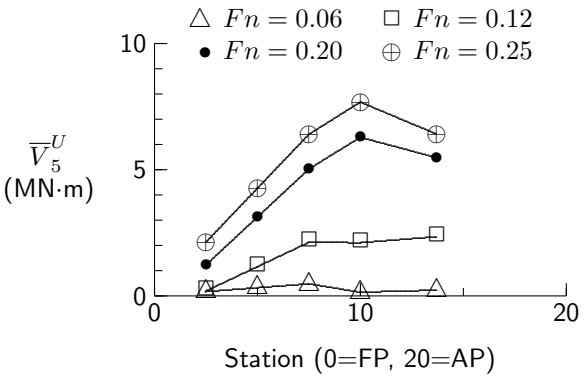

Figure 16: Mean Sag Moment Due to Ship Forward Speed

of 0.12. This bending moment represents the difference between mean sag in waves and mean sag at speed in calm water. The nondimensional mean sag due to waves is generally higher at the lower wave steepness. It should be noted that the experimental error is significantly greater for the mean sag than for the oscillatory bending moment amplitude. The relatively small amplitude and susceptibility to signal drift are suspected to be the primary reasons for experimental error in mean sag values.

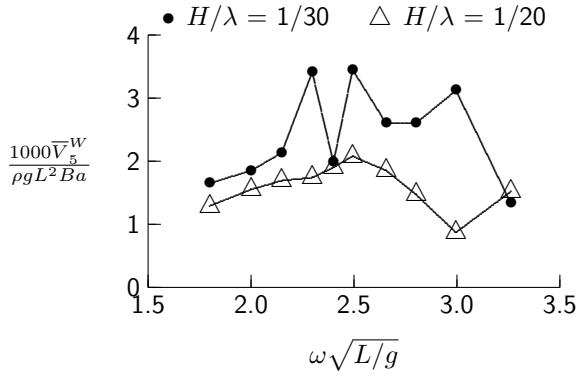

Figure 17: Midships Mean Sag Due to Waves, Head Seas, $Fn = 0.12$

As mentioned previously, the sag/hog ratio indicates the importance of nonlinear effects. The wave-induced sag/hog ratio can be expressed as:

$$\frac{V_5^{sag}}{V_5^{hog}} = \frac{V_5 + \overline{V}_5^W}{V_5 - \overline{V}_5^W} \quad (8)$$

Figure 18 shows the sag/hog ratios based on the above equation and measured values. The computed sag/hog ratios indicate that nonlinear effects are important at both wave steepnesses.

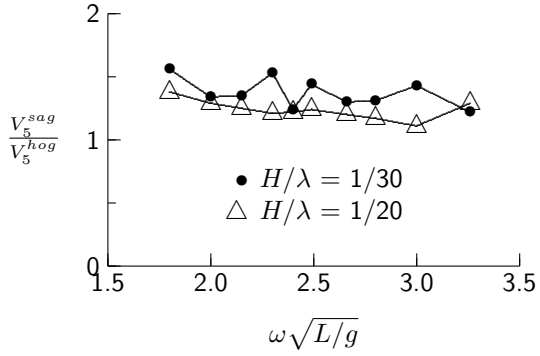

Figure 18: Wave-Induced Sag/Hog Ratio, Head Seas, $Fn = 0.12$

Sag/hog ratios from other researchers provide useful comparisons with the values given in Figure 18. Experimental results for the narrow stern warship model Lloyd et al. [6] show sag/hog ratio increasing to approximately 1.2 as wave steepness H/λ increases to 1/25. No slamming occurred during their model tests.

Clark [1] gives extreme lifetime predictions of maximum midships hog and sag based on full scale measurements. For expected lifetime maximum midships bending moment, the sag/hog ratio ranges between 1.40 and 1.78 for eight different ships. An interesting result from Clark is that derived sag and hog values based on static balance on a trochoidal wave show very good agreement with the extreme values derived from full scale measurements, suggesting that nonlinear effects are very important for hydrostatic forces but less important for other force components in extreme conditions. Although Clark's static balance doesn't include slamming forces, a likely explanation for its good results in extreme conditions is that ship captains usually reduce speed or change heading to avoid slamming in extreme conditions.

Guedes Soares [23] gives a detailed comparison of extreme sag and hog values with linear predictions of vertical bending moment. He includes quadratic frequency domain predictions from Jensen et al. [24], which give sag/hog ratios of 1.32 and 1.52 at Froude numbers of 0.31 and 0.40 respectively for extreme loads on a frigate.

The experimental results for the CPF hydroelastic model are consistent with other reported work which indicates the importance of mean bending moment due to waves and the sag/hog ratio. Although linear theories give good results for oscillatory bending moments, nonlinear approaches are required to determine mean bending moments and sag/hog ratios. Jensen and Dogliani [25] give an example of a quadratic frequency domain method for including nonlinear effects. Their approach is appealing because it is an extension of linear frequency domain theory, which is reliable and computationally efficient. Alternatively, computationally intensive time domain methods (e.g. References 26, 27, and 28) could be used to predict nonlinear effects.

VERTICAL WHIPPING LOADS IN REGULAR WAVES

Whipping loads in regular waves due to the first vertical bending mode were determined using spectral analysis. Vertical responses in the full scale frequency range of 1.1-1.6 Hz were assumed to be caused by whipping in the first bending mode, for which the model has a full scale natural frequency of 1.42 Hz. The natural vertical bending frequency was well above encounter frequencies for regular wave tests, thus permitting separation of non-whipping and whipping components in regular waves.

While spectral analysis yields RMS whipping responses, of greater importance are the maximum whipping responses. For wave-induced motions and loads, the maximum response in regular waves relative to the mean is simply $\sqrt{2}$ times the RMS response. In contrast, the maximum whipping response will occur immediately after a slam and will be followed by damped responses. The following equation based on the assumption of small damping is used to model the whipping vertical bending moment response to a slam occurring at time t_s:

$$V_5^w(t) = \hat{V}_5^w \exp\left[-\xi_w \omega_w (t - t_s)\right] \times \cos \omega_w (t - t_s) \quad \text{for } t \geq t_s \quad (9)$$

where $\hat{V}_5^w$ is the maximum modal whipping moment induced by the slam, ξ_w is the modal damping coefficient, and ω_w is the modal frequency. In the current analysis for regular waves, the whipping response is further idealized by assuming that a slam occurs once per wave encounter and that the response from a given slam becomes negligible after a subsequent slam occurs.

An example is presented using the CPF at a Froude number of 0.12 in head seas with wavelength equal to the ship length. If the wave height is sufficiently high, a new slam will occur once during each wave encounter. Note that the wave encounter period of 6.9 s is much greater than the first natural vertical bending period of 0.70 s, indicating that springing effects will be negligible. Approximately 10 whipping cycles will occur between successive

wave encounters for this case. Figure 19 shows a time series of the idealized whipping response using the measured damping coefficient of 2.7 percent for the first vertical bending mode. While it is assumed that whipping response from a given slam is negligible when a subsequent slam occurs, Figure 19 indicates that the transient response to a slam still has an amplitude of approximately 20 percent of its maximum value after one wave encounter period.

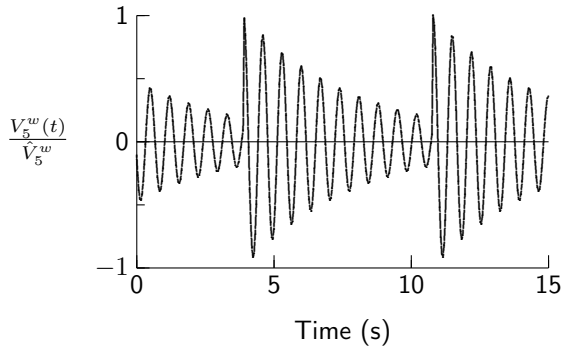

Figure 19: Time History of Idealized Whipping Response in Regular Waves

Using the idealized whipping response of Equation (9), the following expression has been derived for determining the ratio of the maximum whipping response to the RMS whipping response in regular waves:

$$\frac{\hat{V}_5^w}{\text{RMS } V_5^w} = \sqrt{\frac{8\pi\xi_w n_w}{1-\exp\left(-4\pi\xi_w n_w\right)}} \quad (10)$$

where n_w is the number of whipping cycles per wave encounter period, which was taken as being an integer when deriving the above equation. Figure 20 shows ratios of maximum to RMS whipping responses using the damping value of 2.7 percent for the first vertical bending mode. Additional values for damping coefficients of 2 and 3 percent show a moderate sensitivity to damping coefficient. The predicted ratios will approach $\sqrt{2}$ as the damping coefficient approaches zero or the number of whipping cycles approaches zero.

Figures 21 to 24 give experimental whipping and wave-induced vertical bending moments at midships for head seas at Froude numbers of 0.12 and 0.20. As expected, the whipping bending moment response is highly nonlinear with respect to wave amplitude. The nondimensional whipping moment increases significantly with both wave amplitude and ship speed. At the highest wave steepnesses, the magnitude of the maximum whipping moment approaches that

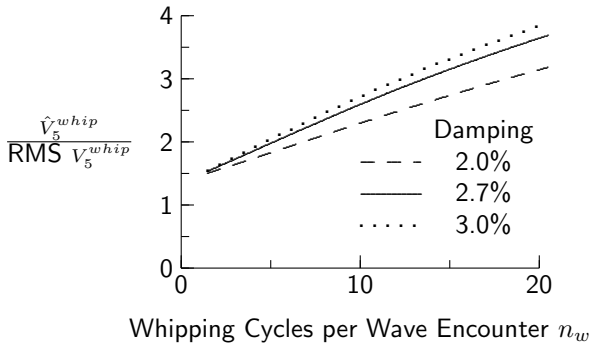

Figure 20: Ratio of Maximum to RMS Whipping Response in Regular Waves for Damped Ship

of the wave-induced moment, indicating the importance of whipping effects in design.

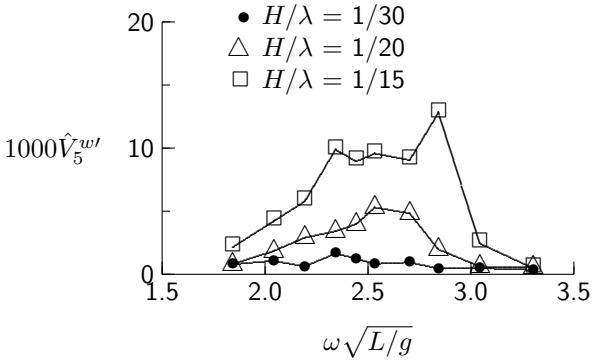

Figure 21: Maximum Whipping Moment at Midships for First Vertical Bending Mode, Regular Head Seas, $Fn = 0.12$

The most relevant source for comparison with the current data are numerical calculations presented by Clarke [1] using revised programs based on the work of Belik et al. [4, 5]. The relevant ships have lengths ranging from 107 m to 125 m and travel in waves with heights of 5 m and wavelengths equal to ship length. For a ship speed of 20 knots, the midships bending moment due to slamming ranges from 23 to 83 percent of the wave-induced bending moment. For the current experimental data at a Froude number of 0.20 (ship speed 14 knots) and nondimensional encounter frequency of 2.5 ($\lambda/L = 1.0$), the ratio of whipping to wave-induced bending moment is 15 percent for a wave steepness of 1/30 ($H = 4.2$ m) and 42 percent for a wave steepness of 1/20 ($H = 6.2$ m). For a Froude number of 0.25 (ship speed 17 knots) and wave steepness of 1/30 ($H = 4.2$ m), the ratio of maximum whipping to wave-induced bending moment is 16 percent. Given

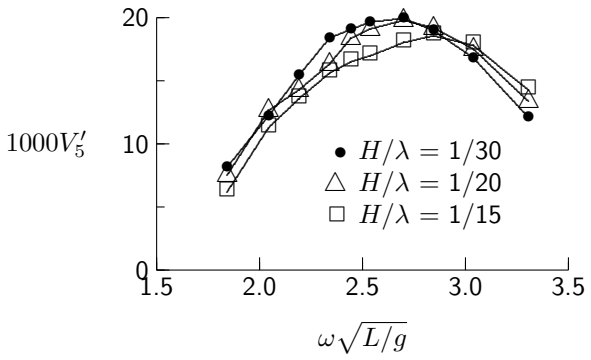

Figure 22: Wave-Induced Vertical Bending Moment at Midships, Regular Head Seas, $Fn = 0.12$

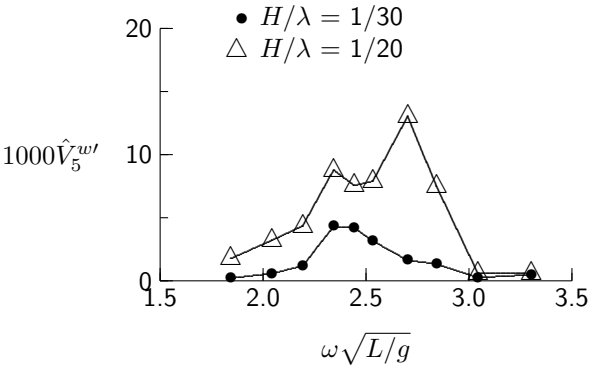

Figure 23: Maximum Whipping Moment at Midships for First Vertical Bending Mode, Regular Head Seas, $Fn = 0.20$

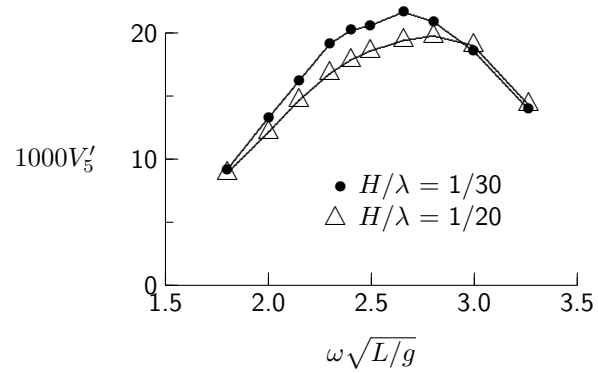

Figure 24: Wave-Induced Vertical Bending Moment at Midships, Regular Head Seas, $Fn = 0.20$

that slamming forces increase with wave height and ship speed, the computed values from Clarke seem consistent with the current experimental values.

The phasing of whipping response relative to wave-induced response is required to predict maximum sagging and hogging moments under slamming conditions. Full scale data for frigates in severe seas [29] show that the maximum whipping moment at midships tends to coincide with the maximum wave-induced sagging moment, thus compounding the importance of whipping loads.

The current whipping response data for regular waves is suitable for validation of slamming and whipping prediction methods such as those presented in References 4 and 5. Unlike slamming data for irregular seas, regular seas data are repeatable and can easily be compared with numerical simulations. Because the maximum whipping responses presented in Figures 21 and 23 are based on an idealization of the whipping response, RMS values rather than maximum values should be used for comparison.

If a time domain simulation method were able to give good predictions of whipping response for the present regular wave data, then it would likely be valid for irregular seas also. Such a method could then be used to predict slamming response in extreme conditions. Computation times would likely be acceptable because ship responses would only have to be evaluated during encounters with waves likely to cause slamming.

CONCLUSIONS

Experiments with a hydroelastic model have provided useful motion and sea load data for a Canadian frigate. The design of six segments attached to an elastic backbone permitted the model to have the required inertial and stiffness properties for shear and bending in horizontal and vertical directions. With the exception of ship roll period, no effort was made to model torsional stiffness and inertial properties.

Model tests in regular waves of steepness 1/30, 1/20, and 1/15 showed that wave-induced ship motions and sea loads were essentially linear. The most noticeable nonlinear trend was a decrease in nondimensional vertical bending for increasing wave steepness. With the exception of torsional moment, linear frequency domain predictions show good agreement with the experiments. For vertical bending moment, strip theory consistently overpredicts while three-dimensional theory using a zero speed Green function gives excellent results at low speed but tends

to overpredict as speed increases. A likely cause of differences between experiments and predictions is the transom stern, which violates slenderness assumptions of strip theory and the present three-dimensional theory at forward speed. The poor agreement between experimental and predicted torsional moments could be partly due to differences between the estimated and actual sectional distributions of roll inertia properties.

Measurements of mean vertical bending moment at midships indicated significant sag caused by the wave profile due to ship forward speed and waves in the seaway. As expected, mean sag moment due to ship forward speed increases with speed. The measured mean sag moment due to regular waves was a significant fraction of the oscillatory moment, leading to sag/hog ratios appreciably greater than unity. Nonlinear methods, including time domain and frequency domain approaches, could be used to predict sag/hog ratios for ship design.

Analysis of whipping-induced accelerations and loads in regular waves was accomplished by analysing response spectra in the vicinity of the first natural vertical bending frequency of the model. This method was possible because the natural model frequency was significantly higher than encounter frequencies of the regular waves. An analytical treatment including damping effects facilitated prediction of maximum whipping response from experimental RMS values. For vertical bending at midships, the maximum whipping moment approaches the wave-induced oscillatory moment as wave steepness and ship speed approach their maximum values.

REFERENCES

[1] J.D. Clarke, "Wave Loading in Warships," in *Advances in Marine Structures* (Dunfermline, 1986), pp. 1–25.

[2] J.J. Jensen and P.T. Pedersen, "Bending Moments and Shear Forces in Ships Sailing in Irregular Waves," *Journal of Ship Research* **25**(4), 243–251 (1981).

[3] A.W. Troesch, "Wave-Induced Hull Vibrations: An Experimental and Theoretical Study," *Journal of Ship Research* **28**(2), 141–150 (1984).

[4] O. Belik, R.E.D. Bishop, and W.G. Price, "On the Slamming Response of Ships to Regular Head Waves," *Transactions, Royal Institution of Naval Architects* **122**, 325–337 (1980).

[5] O. Belik, R.E.D. Bishop, and W.G. Price, "A Simulation of Ship Responses Due to Slamming in Irregular Head Waves," *Transactions, Royal Institution of Naval Architects* **125**, 237–253 (1983).

[6] A.R.J.M. Lloyd, J.C. Brown, and J.F.W. Anslow, "Motions and Loads on Ship Models in Regular Oblique Waves," *Transactions, Royal Institution of Naval Architects* **122**, 21–43 (1980).

[7] A.R.J.M. Lloyd, J.C. Brown, and J.F.W. Anslow, *Wave Induced Motions and Loads on a Model Warship*, Royal Institution of Naval Architects, Occasional Publication No. 3, 1980.

[8] T. Fukasawa, Y. Yamamoto, M. Fujino, and S. Motora, "Motion and Longitudinal Strength of a Ship in Head Sea and the Effects of Nonlinearities," *Naval Architecture and Ocean Engineering* pp. 113–119 (1980).

[9] T.A. Achterides, "Design of Multi-Segmented Models for Springing Experiments," in *PRADS '83 - The Second International Symposium on Practical Design in Shipbuilding* (Tokyo and Seoul, 1983).

[10] S.-K. Chou, F.-C. Chiu, and Y.-J. Lee, "Nonlinear Motions and Whipping Loads of High-Speed Crafts in Head Seas," in *Eighteenth Symposium on Naval Hydrodynamics* (Ann Arbor, 1990), pp. 157–170.

[11] Y. Q. Dong and W. Lin, "Hydroelasticity and Wave Loads for a Full-Form Ship with Shallow Draft," *Journal of Ship Research* **36**(3), 280–285 (1992).

[12] T. Sarpkaya and M. Isaacson, *Mechanics of Wave Forces on Offshore Structures*, Van Nostrand Reinhold, 1981.

[13] E.V. Lewis, "Ship Model Tests to Determine Bending Moments in Waves," *Transactions, Society of Naval Architects and Marine Engineers* **62** (1954).

[14] R.E.D. Bishop and W.G. Price, "On Scaling the Oscillatory Characteristics of Ship Models," *Transactions, Royal Institution of Naval Architects* **123**, 233–252 (1981).

[15] R.E.D. Bishop, J.D. Clarke, and W.G. Price, "Comparison of Full Scale and Predicted Responses of Two Frigates in a Severe Weather Trial," *Transactions, Royal Institution of Naval Architects* **126**, 153–166 (1984).

[16] K.A. McTaggart, "An Improved Strip Theory Program for Ship Motions and Sea Loads in Waves," in *Proceedings of the Fourth Canadian Marine Hydrodynamics and Structures Conference* (Ottawa, June 1997).

[17] N. Salvesen, E.O. Tuck, and O. Faltinsen, "Ship Motions and Sea Loads," *Transactions, Society of Naval Architects and Marine Engineers* **78**, 250–287 (1970).

[18] R.T. Schmitke, "Ship Sway, Roll, and Yaw Motions in Oblique Seas," *Transactions, Society of Naval Architects and Marine Engineers* **86**, 26–46 (1978).

[19] P.D. Sclavounos and C. Lee, "Topics on Boundary Element Solutions of Wave Radiation-Diffraction Problems," in *Fourth International Conference on Numerical Ship Hydrodynamics* (Washington, 1985).

[20] M.S. Chang, "Computations of Three-Dimensional Ship Motions with Forward Speed," in *Second International Conference on Numerical Ship Hydrodynamics* (1977).

[21] Y.H. Kim, F.S. Chou, and D. Tien, "Motions and Hydrodynamic Loads of a Ship Advancing in Oblique Waves," *Transactions, Society of Naval Architects and Marine Engineers* **88** (1980).

[22] J.V. Wehausen and E.V. Laitone, "Surface Waves," *Encyclopedia of Physics* **9**, 446–778 (1960).

[23] C. Guedes Soares, "On the Definition of Rule Requirements for Wave Induced Vertical Bending Moments," *Marine Structures* **124**(3-4), 409–425 (1996).

[24] J.J. Jensen, L. Banke., and M. Dogliani, "Long-term Predictions of Wave-Induced Loads Using a Quadratic Strip Theory," in *International Conference on Ship and Marine Research (NAV '94)* (Rome, October 1994).

[25] J.J. Jensen and M. Dogliani, "Wave-induced Ship Hull Vibrations in Stochastic Seaways," *Marine Structures* **124**(3-4), 353–387 (1996).

[26] R.F. Beck and A.R. Magee, "Time-Domain Analysis for Predicting Ship Motions," in *IUTAM Symposium on the Dynamics of Marine Vehicles and Structures in Waves* (Uxbridge, 1990). Published in 1991.

[27] W.-M. Lin, M. Meinhold, and N. Salvesen, "Prediction of Seakeeping Characteristics of Ships," in *Twentieth Symposium on Naval Hydrodynamics* (Santa Barbara, 1994), pp. 192–213.

[28] H. Bingham, F. Korsmeyer, and J. Newman, "Prediction of Seakeeping Characteristics of Ships," in *Twentieth Symposium on Naval Hydrodynamics* (Santa Barbara, 1994), pp. 19–38.

[29] J.D. Clarke, "Measurement of Hull Stresses in Two Frigates During a Severe Weather Trial," *Transactions, Royal Institution of Naval Architects* **124**, 63–83 (1982).